International Journal of Advanced and Applied Sciences

Journal homepage: http://www.ijaas.in

Laser-Matter Interactions at the Nanoscale: Investigating the Effects on Nanoparticles and Nanotubes

Joshi Megha Bhikulal [1]*, Dr. Abhishek Saxena [2]

[1] *Research Scholar, Department of Physics, Sangam University, Rajasthan, India*
[2] *Associate Professor, Department of Physics, Sangam University, Rajasthan, India*

ARTICLE INFO

Article history:
Received: 11-08-2025
Received in revised form: 10-09-2025
Accepted: 03-10-2025

Keywords:

Laser-matter interaction, nanoparticles, carbon nanotubes, plasmonics, nano scale heating, laser-induced modification, nano photonics, ultrafast lasers, material characterization

ABSTRACT

Laser–matter interactions at the nanoscale have emerged as a critical area of research due to their profound influence on the physical, chemical, and structural properties of nanomaterials. When intense laser irradiation interacts with nanoparticles and nanotubes, it induces localized energy absorption, leading to phenomena such as photothermal heating, melting, reshaping, fragmentation, and phase transformation. These effects are strongly governed by parameters including laser wavelength, pulse duration, fluence, and the intrinsic optical and thermal properties of the nanomaterials. In the case of metallic and semiconductor nanoparticles, laser exposure can result in size redistribution, surface modification, and enhanced plasmonic responses, while carbon-based nanotubes exhibit defect generation, alignment, and controlled functionalization. Understanding these laser-induced processes is essential for tailoring nanomaterials for applications in nanofabrication, sensing, photonics, biomedicine, and energy devices. This study reviews and investigates the fundamental mechanisms underlying laser–nanomaterial interactions and highlights recent advances in controlled modification of nanoparticles and nanotubes through laser processing techniques.

Introduction

These lasers' superior mechanical qualities and wide lasing bandwidth outweighed the drawbacks of dye-based lasers. In addition to their enormous strength, ultrashort laser pulses have femtosecond durations, which allow them to interact with matter in a wide range of ways. Strickland and Mourou proposed the chirp pulse amplification (CPA) technology, which significantly increased peak output from 100 watts to terawatts. Following the discovery of CPA, lasers based on Kerr-lens-mode-locking the tiny table top Terawatt steady Ti: sapphire laser became accessible.

The Advance Photonic Research Institute (APRI) of Korea created a CPA-based Ti: sapphire laser system in 2010 with a pulse length of 30 femtoseconds and a 1-Petawatt level. Peak power of about 200 Petawatts and intensities of up to 1021 W/cm2 were attained by Jeong and Lee. Large-scale high-power laser systems are still being developed at a number of facilities worldwide. The University of Rochester's Laboratory for Laser Energetics uses an OMEGA system with a 60-laser beam. The 192-laser beam system at Lawrence Livermore National Laboratory is part of the National Ignition Facility (NIF), the biggest laser system in the world.

Plasma modes

Plasma supports a wide range of electrostatic and electromagnetic modes and displays collective behaviour of free electrons and ions. Two electrostatic (longitudinal) waves are supported by an magnetized plasma: a high frequency electron plasma wave, often known as a Langmuir wave, and a low frequency ion acoustic wave.

Instabilities that are parametric

The intriguing phenomena of stimulated Raman scattering stimulated Brillouin scattering, two-plasmon decay, decay instability, modulational instability, filamentation instability, and oscillating two stream instability are all caused by the parametric coupling between these modes. Here, I go over three of these crucial procedures that are pertinent to the current research.

Raman scattering stimulation

In Stimulated Raman Scattering (SRS), a high power laser (pump) of frequency ω_0 and propagation wave vector $\vec{k}_0$ excites a Langmuir wave at $(\vec{\omega}k)$ and a scattered electromagnetic wave (sideband). It occurs at plasma densities (n_0^0) below one-fourth of the critical density (n_{cr}) corresponding to the pump. The frequency and wave vector of the scattered wave (ω_1,$k1$) are the difference of frequencies and wave vectors of the pump and the Langmuir wave (corresponding to the conservation of energy and momentum)

$\omega 1 = \omega 0 - \omega$, and $\vec{k}1 = \vec{k}0 - \vec{k}$.

Numerous groups have thoroughly investigated SRS in homogeneous and inhomogeneous plasmas both theoretically and practically with the application to laser pallet irradiation, beginning with the groundbreaking work by Liu et al. and Forslund et al. In their investigation of the SRS process in a gas jet plasma with submicron-sized clusters, Tiwari and Tripathi found a significant increase in growth rate. In the presence of periodically spaced nanoparticles, Parashar investigated SRS using collective modes. The impact of laser-driven cluster coulomb explosion on SRS was examined by Tiwari et al. Enhancement Raman scattering in a series of vertical silicon nanowires was investigated by Huang et al. The usefulness of SRS in the bulk and nanoscale regimes has been examined by Prince et al.

The Langmuir waves can Landau damp on electrons and have phase velocities that are similar to a few times the thermal velocity of an electron. TPD is hence a source of hot electron production. TPD has been identified as a significant problem for laser-driven fusion and can compete with SRS at quarter critical density.

Ikemura and Mima used a two-dimensional laser pump to investigate the TPD in a self-induced plasma channel. Sharma and Tripathi performed the TPD analysis in a cylindrical shape using a perturbative technique to eliminate convective losses for Langmuir wave propagation. In the nonlinear stage of TPD, Yan et al. conducted simulation tests and found considerable laser absorption and hot electron production. A thorough investigation of TPD in inhomogeneous plasmas pertinent to the inertial confinement goals was conducted by Wen et al.

Interaction between laser clusters

High-density solids and low-density gases have been the subject of successful experiments in high power laser-matter interaction throughout the last few decades. These two goals have certain problems. Gas targets have low laser absorption, which results in a low conversion efficiency to harmonics, whereas solid targets produce debris that negatively affects optics. By combining the advantageous effects of solid and gaseous phases, cluster targets provide an effective medium of interaction. When clusters are exposed to a laser, they effectively absorb the laser's energy and transform into plasma balls that interact with the laser resonantly when the laser's frequency matches the frequency of the cluster's electron cloud's space charge oscillations with respect to the ions (a phenomenon known as surface plasmon resonance).

The development of clusters in the broad clustering region by the flow of cooled gas at high pressure into vacuum was investigated experimentally by Hagena and Obert, who observed that the cluster gas's distinctive dependency on backing pressure, temperature, and nozzle geometry. The hydrodynamic nano-plasma model, which treats clusters as spherical plasmas, was introduced by Ditmire et al. in 1996 and is the most intriguing and effective model for cluster formation. A collisionless theoretical model for the ion coulomb explosion of clusters by lasers with a Gaussian intensity profile was created by Liu and Tripathi.

Plasmon resonance on the surface

Surface plasmon resonance is a unique property of planar vacuum-metal interfaces or surfaces loaded with metallic nanoparticles or nanotubes, and it has been discovered to be a useful diagnostic tool for increased Raman scattering. The entire absorption of incident electromagnetic waves on nanoscale or microscale structures has been investigated by a number of organizations both theoretically and empirically, as well as a comparison of embedded surfaces with smooth metal surfaces. The space charge oscillation of the electron cloud is caused by the anomalous absorption of surface plasma waves across the metal surfaces embedded with metallic nanoparticles, which creates an electric field in the nanoparticles.

Literature review

Kharphanbuh et al. (2025) [1] investigate the impact of manganese (III) oxide nanoparticles produced via pulsed laser ablation in liquids on protein stability and folding mechanisms. Their study provides critical insights into nanoparticle protein interactions, demonstrating that laser-generated Mn_2O_3 nanoparticles can induce protein misfolding through surface-mediated oxidative stress and conformational disruption. This work is significant in the context of nanotoxicology, as it highlights potential biological risks associated with metal oxide nanoparticles synthesized through physical methods. The findings contribute to understanding the molecular-level implications of nanoparticle exposure in biomedical and environmental systems.

Kharphanbuh and Nath (2025) [2] explore an innovative approach for the recovery of valuable metals such as gold and tantalum from electronic waste using underwater laser-assisted processing combined with external electric fields. The study emphasizes a sustainable and

selective metal extraction strategy that minimizes chemical usage and environmental contamination. By integrating laser–matter interaction with electro-assisted separation, the authors demonstrate improved recovery efficiency and material purity. This work contributes to the growing field of green recycling technologies and underscores the potential of laser-based techniques in circular economy applications.

Sohail (2025) [3] presents a comprehensive overview of recent progress in nanomaterials, covering synthesis techniques, characterization methods, and emerging applications. The review highlights advancements in physical, chemical, and green synthesis routes, with particular emphasis on tailoring nanostructures for biomedical, electronic, and energy-related applications. By systematically summarizing current trends and challenges, the study serves as a valuable reference for researchers seeking to understand the evolving landscape of nanotechnology and its interdisciplinary applications.

Kirubakaran et al. (2025) [4] provide an extensive review of green synthesis approaches for nanoparticle fabrication, focusing on advancements in biomedical and environmental applications. The authors discuss plant-, microbe-, and biomolecule-mediated synthesis routes, emphasizing their eco-friendly nature, cost-effectiveness, and scalability. The review also evaluates the functional performance of green-synthesized nanoparticles in drug delivery, antimicrobial activity, catalysis, and pollutant remediation. This work reinforces the importance of sustainable nanomanufacturing and positions green synthesis as a viable alternative to conventional chemical methods.

Dubey et al. (2025) [5] examine the chemical integration of biodegradable materials for energy storage applications, targeting sustainable environmental solutions. Their study focuses on the structural and functional optimization of eco-friendly materials designed for use in next-generation energy devices. By addressing material compatibility, degradation behavior, and performance efficiency, the authors highlight the role of molecular-level engineering in developing sustainable energy storage systems. This work bridges nanomaterials science with environmental sustainability and energy research.

Zango et al. (2025) [6] present a state-of-the-art review focusing on the green synthesis and surface modification of zinc oxide (ZnO) nanoparticles for environmental remediation applications. The authors critically analyze eco-friendly synthesis routes, including plant-mediated and biogenic approaches, emphasizing their role in reducing toxicity and improving sustainability. The review further discusses structural and electronic modifications of ZnO nanoparticles that enhance their photocatalytic efficiency for organic pollutant degradation and CO_2 conversion. This study highlights the dual environmental benefit of ZnO-based nanomaterials in pollution control and carbon mitigation technologies.

Naveed et al. (2025) [7] provide a comprehensive evaluation of heavy metal-based nanoparticles used in cosmetic formulations, addressing both functional benefits and toxicological concerns. The review examines commonly employed nanoparticles such as titanium dioxide, zinc oxide, silver, and gold, focusing on their roles in UV protection, antimicrobial activity, and product stability. Importantly, the authors discuss dermal penetration, bioaccumulation, and potential ocular and systemic toxicity associated with prolonged exposure. This work contributes significantly to the discourse on consumer safety and regulatory frameworks in nanocosmetics.

Sahu and Tiwari (2024) [8] offer an in-depth discussion on carbon allotropes, covering their fundamental structures, synthesis techniques, characterization methods, and functionalization strategies. The chapter systematically explores various carbon forms, including graphene, carbon nanotubes, fullerenes, and emerging allotropes, highlighting their unique physicochemical properties. The authors also emphasize surface functionalization as a key factor in tuning carbon materials for applications in electronics, energy storage, and biomedicine. This contribution serves as a foundational reference for researchers working in carbon-based nanomaterials.

Ullah et al. (2024) [9] theoretically investigate tolanene, a newly proposed two-dimensional carbon allotrope featuring sp–sp² hybridization. Using advanced computational modeling, the authors analyze the structural stability, electronic band structure, and potential mechanical properties of this novel material. Their findings suggest that tolanene exhibits promising electronic characteristics, making it a potential candidate for nanoelectronic and optoelectronic applications. This study expands the landscape of 2D carbon materials and provides theoretical guidance for future experimental synthesis.

Liu et al. (2024) [10] comprehensively review carbon nanotubes (CNTs), emphasizing their structural features, synthesis methods, and catalytic applications. The authors discuss various CNT production techniques, including chemical vapor deposition and arc discharge, along with purification and functionalization strategies. Special attention is given to the role of CNTs in carbon-based catalysis, where their high surface area and electronic conductivity enhance catalytic performance. This chapter underscores the versatility of CNTs as key components in advanced catalytic and energy-related systems.

De Albornoz-Caratozzolo and Cervantes-Sodi (2024) [11] introduce the concept of *Chiraltube*, a computational and theoretical framework for rolling two-dimensional materials into chiral nanotubes. Their study systematically explains how chirality can be engineered by controlling rolling vectors, extending beyond conventional carbon nanotubes to a wider class of 2D materials. The work provides valuable insights into structure–property relationships, showing how chirality influences electronic and mechanical behavior. This contribution is significant for the rational design of next-generation chiral nanomaterials for nanoelectronics and optoelectronics.

Hughes et al. (2024) [12] present a comprehensive review of carbon nanotube (CNT) research, covering material synthesis, characterization techniques, and emerging applications. The authors discuss advancements in scalable manufacturing, defect control, and functionalization strategies that improve CNT performance. Emerging applications in energy storage, flexible electronics, sensors, and biomedical devices are critically examined. This review highlights the continued relevance of CNTs as multifunctional nanomaterials while addressing challenges related to commercialization and material uniformity.

Shah et al. (2024), [13] in their ACS Omega publication, investigate advanced nanomaterial systems with a focus on structure–property correlations, although the specific title details are not provided. The study contributes to understanding how compositional and morphological tuning at the nanoscale affects functional performance. Their work aligns with contemporary research trends emphasizing application-driven nanomaterial optimization, particularly in sensing and electronic platforms.

Aalam et al. (2024) [14] explore nanostructured material systems in ACS Omega, emphasizing surface engineering approaches to enhance material sensitivity and selectivity. Their research underscores the importance of surface modification and porosity in improving interaction with target analytes. This work forms part of a broader effort to develop high-performance nanomaterial-based sensors through controlled structural design.

Aalam et al. (2024) [15] specifically report the development of a highly sensitive surface-modified porous carbon nanotube-based sensor for ammonia gas detection. The study demonstrates that surface functionalization significantly enhances gas adsorption and charge transfer, leading to improved sensor response at low ammonia concentrations. This work contributes to the advancement of CNT-based gas sensors for environmental and industrial monitoring.

Aalam et al. (2024) [16] further investigate ammonia sensing using porous multiwalled carbon nanotubes decorated with manganese nanoparticles. Their results reveal that the concentration of Mn plays a critical role in tuning sensitivity, selectivity, and response time. The study highlights synergistic effects between CNTs and metal nanoparticles, providing a pathway for optimizing hybrid nanocomposites for gas sensing applications.

Verma and Kumar (2024) [17] study the gas sensing behavior of copper-doped polyaniline (PANI) nanocomposites toward ammonia detection. The authors show that Cu doping enhances conductivity and gas adsorption efficiency, resulting in improved sensing performance at room temperature. This work demonstrates the potential of polymer–nanocomposite systems as cost-effective alternatives to conventional metal oxide sensors.

Deena et al. (2024) [18] investigate the nonlinear optical absorption and optical limiting properties of bismuth-based binary and ternary nanostructures. Their findings reveal strong nonlinear behavior, attributed to electronic transitions and defect-induced states within the nanostructures. This study highlights the potential of bismuth-based nanomaterials for photonic and laser protection applications.

Nangare and Patil (2023) [19] provide a critical review of black phosphorus nanostructure-based surface plasmon resonance (SPR) sensors for biological and chemical detection. The

authors discuss synthesis challenges, surface stability, and sensing mechanisms, emphasizing the exceptional sensitivity and selectivity of black phosphorus. This review positions black phosphorus as a promising material for next-generation plasmonic sensing technologies.

Hooshmand et al. (2023) [20] review wearable nano-based gas sensors designed for environmental monitoring. The study examines flexible nanomaterials, device architectures, and integration strategies suitable for wearable platforms. Challenges related to power consumption, long-term stability, and signal reliability are critically discussed. This review underscores the growing importance of wearable nanotechnology in real-time environmental and health monitoring.

Methodology

Absorption with nonexpanding nanoparticles

Consider a metal surface of thickness D, embedded with the metallic nanoparticles of radius c r and interparticle separation d. An interface separates the metal surface with free space, with z > 0 as free space and z < 0 metal. A p-polarized laser is incident on the interface at an angle θ, with electric and magnetic fields represented as

$$E_i = A\left(\frac{(x+sin\theta)}{cos\theta}\ z\right)e^{-i}\left(\omega t - \frac{\omega}{c} sin\theta x + \frac{\omega}{c} cos\theta\ z\right) \quad (1)$$

$$H_{iy} = \frac{(k \times Ei)y}{\mu_0 \omega} = \frac{A}{\mu_0\, c\, cos\theta} e^{-i}\left(\omega t - \frac{\omega}{c} sin\theta x + \frac{\omega}{c} cos\theta\ z\right) \quad (2)$$

where μ0 is the magnetic permeability of the free space.

The electric field and magnetic field of the laser, reflected from the metal surface is

$$E_R = AT_A\left[x - \frac{sin\theta}{cos\theta} z\right] e^{-i}\left(\omega t - \frac{\omega}{c} sin\theta x + \frac{\omega}{c} cos\theta\ z\right) \quad (3)$$

$$H_{RY} = \frac{(k \times E_R)y}{\mu_0\, \omega} = -\frac{AR_A}{\mu_0\, c\, cos\theta} e^{-i}\left(\omega t - \frac{\omega}{c} sin\theta x + \frac{\omega}{c} cos\theta\ z\right) \quad (4)$$

The transmitted electric field and magnetic field of laser inside the metal is

$$E_T = AT_A\left[x + \frac{sin\theta}{k_z\ c\backslash\omega} z\right] e^{-i(}\omega t - \frac{\omega}{c} sin\theta x + k_z z),$$

$$H_{TY} = \frac{AT_A}{\mu_0 \omega} \left\{ k_z + \frac{\omega^2}{c^2} \frac{sin\theta}{k_z} \right) e^{-i(} \omega t - \frac{\omega}{c} sin\theta x + k_z z), \quad (5)$$

where $\left\{ (k_z + \frac{\omega^2}{c^2} \frac{sin\theta}{k_z} \right)$ is the z component of the propagation vector and m ε is the permittivity of the metal.

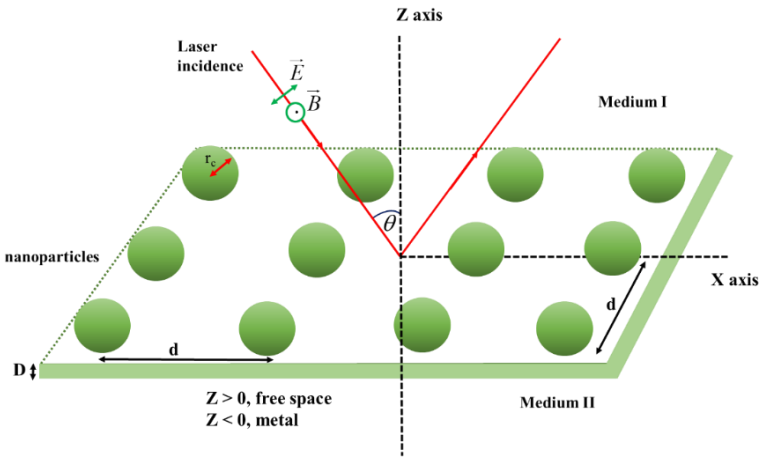

Figure 1: shows a schematic of an oblique laser incidence on a metal surface that has nanoparticles implanted in it with radius rc and interparticle spacing d.

Applying the boundary conditions and condition of continuity, of electric and magnetic field, at the interface

(at z = 0),

we have By the continuity of E x electric field, we have

A AR AT + = A A , 1 . + = R T A A

By the continuity conditions of magnetic field

H H J yI yII sx − =

We have evaluated this expression for the following parameters: 15 ω = ×2 10 sec rad , 9 2 10 c r m − = × , r d c = 0.1, and 2 υ ω 10− = . The self-consistent inclusion of absorption on amplitude transmission coefficient TA reduces the absorption coefficient by a factor of 2.1. the variation of

absorption coefficient with the normalized laser frequency for different values of θ. the variation of absorption coefficient with angle of incidence θ, for different values of the laser frequency. The value of the absorption coefficient is found to be maximum at the resonance frequency.

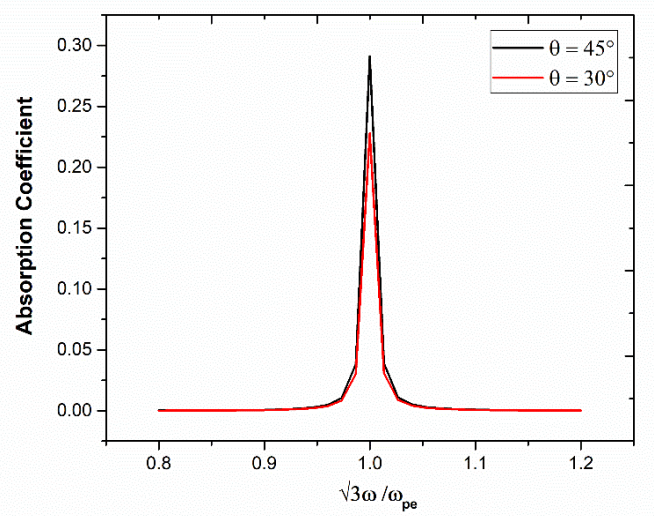

Figure 2: shows the fluctuation of the absorption coefficient for nanoparticles as a function of normalized laser frequency for various angles of incidence θ = 45°, 30°, and the following parameters: r = 2 ×109 m, r d } 0.1, and $^{5\ 7}$ = 102.

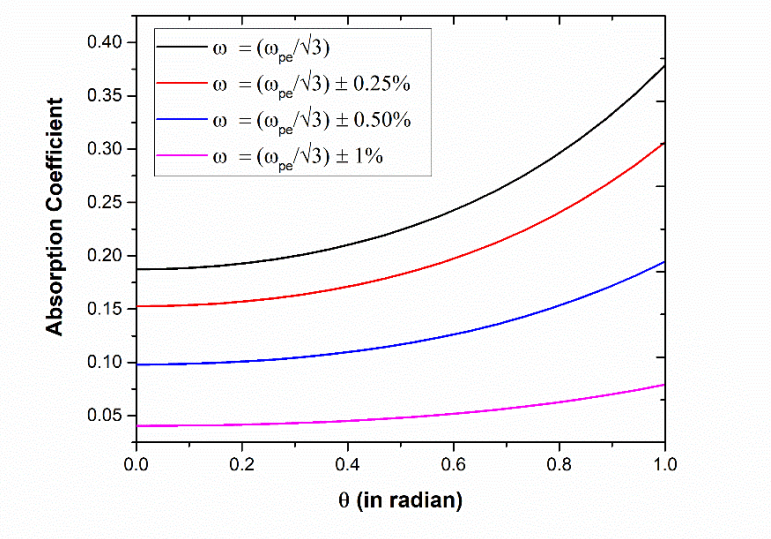

Figure 3: Absorption coefficient variation for the nanoparticles as a function of angle of incidence θ, for different laser frequencies of: (3), (3) 0.25%, (3) 0.50%, ω ω ω ω ω ω = = ± = ± pe pe pe and (3) 1%. ω ω = ±

The large partial pressure of heated electrons causes the ion coulomb explosion, by leaving behind the positive ion core, and results in the expansion of core at the rate of ion sound speed, 1/2 ( ) s e i c T m = . The increase in the radius of nanoparticle with time can be given as

0 0 t c c s r r c dt = + ∫ ,

where c0 r is the radius of the unexpanded nanoparticle. As the radius of the nanoparticle increases due to the core expansion, the electron density decreases, in order to keep the term 2 3 pe c ω r constant. Therefore,

2 3 2 3 0 0 , pe c pe c ω ω r r

We have evaluated Eqs. (3) and (4) for the following set of parameters: 15 ω = ×2 10 sec, rad 0 2 5 c r nm = – , 0 0.1 0.3 c r d = – , 2 0 υ ω 10– = and 2 2 2 0 e E m T (3) 4 6 ω = – . the variation of T T e 0 as a function of normalized time 0 υ t (for 12 1 0 0 υ υ 10 sec , 1 t – = = corresponds to 1ps) for the different values of the initial nanoparticles radius and laser intensity.

Absorption with nonexpanding CNTs Consider an assembly of CNTs mounted on the metal-free space interface (0) z = of thickness D, with z > 0 as free space and z < 0 metal. The assembly comprises of Nc CNTs per unit area placed parallel to each other with axes along z ˆ and

separation between the CNT axes is d. The CNTs have interior free electron density e0, n radius rc and length L A p-polarized laser is incident on the interface at an angle θ, with electric and magnetic fields represented as For the case of CNTs, we can derive the expression for the excursion and velocity in a similar manner as in the case of spherical nanoparticles on a metal surface, by replacing 3 ωpe with 2 ω pe .

We have evaluated this expression for the following parameters: 15 ω = ×2 10 s rad , 9 2 10 , c r m – = × 0.002, c r d = L d = 0.8, and 2 υ ω 10– = . The self-consistent inclusion of absorption on amplitude transmission coefficient TA reduces the absorption coefficient by a factor of 2.2. variation of absorption coefficient with the normalized laser frequency for different values of θ. The absorption is resonantly enhanced, when the applied frequency is in resonant with the plasmon frequency of the CNTs, i.e., ω tends to 2 and results in the strong absorption of laser energy. variation of absorption coefficient with angle of incidence θ, for different values of the laser frequency. One may recognize that the absorption discussed in this section is valid at low intensity as the effects of heating of electrons and expansion of CNTs have been ignored. This is known as linear absorption

Result Analysis

The laser absorption on metal surfaces, embedded with nanoparticles and nanotubes, is strongly enhanced by the plasmon resonance. The effect of laser absorption, in both the case of nanoparticles and CNTs, is explicit in the amplitude transmission coefficient TA that eventually modifies and reduces the absorption coefficient. The absorption coefficient has a sharp peak at surface plasma resonance, 3 ω ω= pe, for nanoparticles and 2 ω ω= pe for CNTs. As one increases the angle of incidence, the absorption peak increases. For the expanding clusters, near the plasmon resonance, the heating rate is maximum that leads to the sharp peak in electron temperature. However, the heating term later weakens and the electron temperature falls due to thermal conduction. The temperature rises sharply close to resonance time R t , for a given nanoparticle radius. Due to the slow expansion rate of the bigger nanoparticles, the resonance is delayed. The enhancement in laser intensity leads to higher electron temperature. In this case, resonance is achieved at an earlier stage. The absorption coefficient also acquires a maximum value at R t.

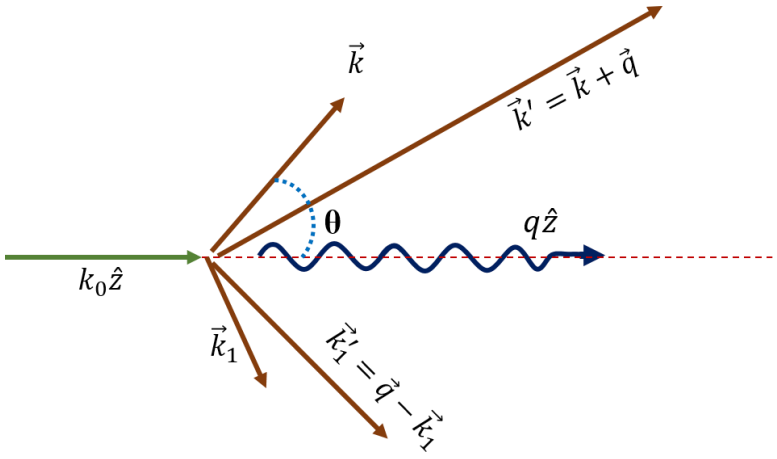

Figure 4: Schematic of two-plasmon decay process.

The small radius nanoparticles are found to attain the saturation at lower values in comparison with bigger nanoparticles. Similar, effects are observed in the case of CNTs. The present treatment is valid for the CO2 laser as well. However, plasmon resonance effects will appear much later in time, when the electron density has fallen to a very low value to reach plasmon resonance at 2 ω ω= pe . The present study has important applications in the field laser based ion acceleration processes.

In the nonlinear coupling, we may ignore the thermal corrections in , , L k vω , , L nω k 1 1 , , L k vω and 1 1 , . L k nω in Eqs. (5). The pump 0 0 (,) ω k and Langmuir wave 1 1 (,) ω k exert difference frequency Ponderomotive force on the plasma electrons at (,) ω k , , , , F e p k ω ϕ p k ω → ≡ ∇ (5.8) where, 1 1 0 1 0 , , 0 1 0 1 . . 2 2 k p k e E E e E m m ω ω ϕ ϕ ω ω ω ω ∗ ∗ ∗ ∇ = − = is the ponderomotive potential. The potential p k ω, ϕ and ϕω,k imparts the oscillatory velocity to the electrons, , , , ( ) . k k p k v e k m ω ω ω ϕ ϕ ω + = − (5.9) However, in the presence of density ripple, the electron velocity component at (,) ω k couples with the stationary electron density ripple, in order to produce an electron density perturbation , k nω ′ at 0 (,) ω k k q ′ = + that generates a third Langmuir wave of potential ϕω, k ′ . Using equation of continuity, the density perturbation , k nω ′

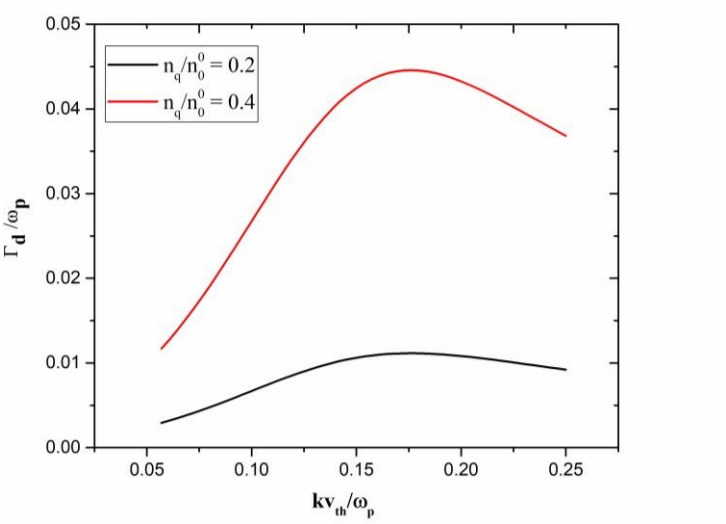

Figure 5: Variation of damping rate ( ) Γd p ω with normalized wave number ( ) th p kv ω of primary Langmuir wave, in rippled density plasma 0 0 ( ) q n n = 0.2, 0.4.

The right hand side of Eq. (7) represents the nonlinear coupling between the pump and Langmuir scattered wave. The effect of the density ripple on the primary Langmuir wave is visible in third term of Eq. (8). Similarly, for the Langmuir wave 1 1 (,) ω k , the electron velocity component at 1 1 (,) ω k couples with the stationary electron density ripple, in order to produce an electron density perturbation 1 1 , k n ω ′ at 1 1 0 1 (,) ω k q k ′ = – that generates a Langmuir wave of potential 1 1 ω , k ϕ ′ .

We have calculated the damping rate for the following parameters: 0.3, th p qν ω = ( ) 0.05, th ν c = 0 1.7 p k c = ω , 0 θ = 45 , and 0 0 0.2,0.4 q n n = . the variation of normalized damping rate with normalized wave number of the Langmuir wave. As the wave number increases, the damping rate rises, acquires a broad maximum and falls off gradually. The damping rate nearly scales as the square of ripple density. At 0 0 0.2 q n n = , the damping rate is 0.01 and at 0 0 0.4 q n n = , this becomes 0.04 for ( ) 0.15 th p kv ω = . The damping rate becomes approximately four times with the twice in the number density of ripples.

Growth rate

In the presence of laser, R.H.S. of Eq. (9), is finite and the two Langmuir waves are nonlinearly coupled. Expanding $\in\omega$,k and , 1 1 ω k ∈ around the resonant frequencies, that is, taking

1 1 1 1 , , , , 1 1 ( ) , ( ) , k k k k d d i i ∈ = Γ + Γ ∂ ∈ ∂ ∈ = Γ + Γ ∂ ∈ ∂ ω ω ω ω ω ω one obtains from Eq. (7)

If we ignore the contribution of the density ripple on the coupling coefficient i.e. on the R.H.S. of Eq. (3), we have

We have solved Eq. (7) for the following parameters: 0 0 0 0 0 , | | k a eE m c c ≡ = = ω ν ω 0.03, 0.05, th p qν ω = 0.3, ( ) 0.05, th ν c = 0 1.7 p k c = ω , 0 θ = 45 , and 0 0 0,0.2,0.4 q n n = . Figure 5.3 shows the variation of normalized growth rate ( ) Γ ω p with normalized wave number ( ) th p kv ω of Langmuir wave for the normalized laser amplitude 0 0 0 0 0 , | | k a eE m c c ≡ = = ω ν ω 0.05. The growth rate increases with the increase of propagation vector.

The presence of density ripple in plasma significantly enhances the threshold laser intensity for two-plasmon decay and leads to the reduction in the growth rate of the parametric instability. In the absence of ripple, TPD occurs at all values of k. The parametric instability does not occur at lower value of k upto k = km. The minimum value of wave number km at which growth begins, increases with 0 q 0 n n . At 0 0 0.2, q n n = growth begins at 0.08 and for 0 0 0.4 q n n = , the growth rate begins at 0.12 th p kv ω > . The magnitude of growth rate decreases with corresponding increase in ripple density. In the parametrically unstable regime, the growth rate falls with 0 q 0 n n . Typically, at 0 0 0.2 q n n = the growth rate is 0.01 while for 0 0 0.4 q n n = the growth rate found to 0.004 for 0.15 th p kv ω .

Conclusion

Laser–matter interactions at the nano scale play a pivotal role in determining the structural, optical, and functional properties of nanoparticles and nanotubes. The highly localized energy deposition produced by laser irradiation leads to a variety of physical and chemical processes, including photothermal heating, plasmonic excitation, defect formation, phase transformation, and morphological modification. These effects are strongly dependent on laser parameters such

as wavelength, pulse duration, and fluence, as well as on the intrinsic properties of the nanomaterials.

The investigation of laser-induced effects on nanoparticles and nanotubes demonstrates that laser processing is an efficient and controllable technique for tailoring nanomaterial characteristics without the need for complex chemical treatments. By carefully optimizing irradiation conditions, it is possible to achieve precise control over size, shape, surface structure, and electronic behavior, enabling customized material performance. Overall, understanding laser–matter interactions at the nanoscale not only advances fundamental knowledge of light–matter coupling but also supports the development of innovative applications in nanofabrication, sensing, photonics, biomedicine, and energy technologies.

Reference

1. S. M. Kharphanbuh, K. Baruah, A. S. Roy, and A. Nath, "Protein misfolding by manganese (III) oxide nanoparticles generated by pulsed laser ablation in liquids," *Journal of Molecular Liquids*, vol. 417, Art. no. 126670, 2025.
2. S. M. Kharphanbuh and A. Nath, "Recovery of gold and tantalum from electronic waste using underwater laser-assisted processing in external electric fields," *Journal of Laser Applications*, vol. 37, no. 2, Art. no. 022005, 2025.
3. A. Sohail, "Progress in nanomaterials: Synthesis, characterization, and applications," *Next Nanotechnology*, vol. 8, Art. no. 100263, 2025. **DOI:** https://doi.org/10.1016/j.nxnano.2025.100263
4. D. Kirubakaran *et al*., "A comprehensive review on the green synthesis of nanoparticles: Advancements in biomedical and environmental applications," *Biomedical Materials & Devices*, 2025.
5. S. Dubey, A. Sharma, K. Kaur, K. Pal, M. E. A. Mohsin, and S. Mousa, "Novel chemical integration of biodegradable energy storage materials utilizations for sustainable environment," *Journal of Molecular Structure*, vol. 1345, 2025.
6. Z. U. Zango *et al*., "A state-of-the-art review on green synthesis and modifications of ZnO nanoparticles for organic pollutants decomposition and CO_2 conversion," *Journal of Hazardous Materials Advances*, vol. 17, 2025.

7. M. Naveed *et al*., "Applications of heavy metal-based nanoparticles in cosmetics: A comprehensive review," *Cutaneous and Ocular Toxicology*, vol. 44, no. 1, pp. 1–15, Jan. 2025.
8. S. Sahu and S. Tiwari, "Carbon allotropes: Fundamental, synthesis, characterization, and properties functionalization," in *Carbon Allotropes*, Boca Raton, FL, USA: CRC Press, 2024, pp. 41–70.
9. S. Ullah, M. G. Menezes, and A. M. Silva, "Theoretical characterization of tolanene: A new 2D sp–sp² hybridized carbon allotrope," *Carbon*, vol. 217, Art. no. 118618, 2024.
10. Z. Liu, G. Xiang, C. Yi, and Q. Zhang, "Carbon nanotubes," in *Carbon Catalysis*, Boca Raton, FL, USA: CRC Press, 2024, pp. 251–301.
11. J. M. de Albornoz-Caratozzolo and F. Cervantes-Sodi, "Chiraltube, rolling 2D materials into chiral nanotubes," *Nanoscale Advances*, vol. 6, no. 1, pp. 79–91, 2024. **doi:** https://doi.org/10.1039/D3NA00301A
12. K. J. Hughes, K. A. Iyer, R. E. Bird, J. Ivanov, S. Banerjee, G. Georges, and Q. A. Zhou, "Review of Carbon Nanotube Research and Development: Materials and Emerging Applications," *ACS Applied Nano Materials*, vol. 7, no. 16, pp. 18695–18713, 2024. **doi:** https://doi.org/10.1021/acsanm.4c02721
13. M. A. Shah, M. Sarvar, M. Sadiq, and J. Ali, "(Title not provided)," *ACS Omega*, vol. 9, pp. 4486–(end page not provided), 2024.
14. S. M. Aalam, M. Sarvar, M. Sadiq, and J. Ali, "(Title not provided)," *ACS Omega*, vol. 9, no. 4, pp. 4486–4496, 2024.
15. S. M. Aalam, M. Sarvar, M. Sadiq, and J. Ali, "A highly sensitive surface-modified porous carbon nanotube-based sensor for ammonia gas detection," *ACS Omega*, vol. 9, no. 4, pp. 4486–4496, 2024.
16. S. M. Aalam, M. Sarvar, M. Sadiq, M. N. Bhat, M. Tomar, and J. Ali, "Enhanced ammonia gas sensing properties in porous multiwalled carbon nanotubes decorated with metal nanoparticles: the impact of concentration of Mn," *Advances in Natural Sciences: Nanoscience and Nanotechnology*, vol. 16, no. 1, Art. no. 015003, 2024.
17. A. Verma and T. Kumar, "Gas sensing properties of a Cu-doped PANI nanocomposite towards ammonia," *Materials Advances*, vol. 5, no. 18, pp. 7387–7400, 2024.

18. D. M. Deena, S. Arockia Anushya, A. Dhanusha, T. C. Sabari Girisun, and A. Philominal, “Peculiar nonlinear optical absorption and optical limiting behaviors of bismuth-based binary and ternary nanostructures,” *Diamond and Related Materials*, vol. 141, Art. no. 110656, 2024. **doi:** https://doi.org/10.1016/j.diamond.2023.110656
19. S. Nangare and P. Patil, “Black phosphorus nanostructure based highly sensitive and selective surface plasmon resonance sensor for biological and chemical sensing: a review,” *Critical Reviews in Analytical Chemistry*, vol. 53, no. 1, pp. 1–26, 2023.
20. S. Hooshmand, P. Kassanos, M. Keshavarz, P. Duru, C. I. Kayalan, İ. Kale, and M. K. Bayazit, “Wearable nano-based gas sensors for environmental monitoring and encountered challenges in optimization,” *Sensors*, vol. 23, no. 20, Art. no. 8648, 2023.